Albuquerque Academy Team 1 Understanding 3D Printing Through Atomistic Polylactic Acid Segmental Dynamics Analysis

New Mexico
Supercomputing Challenge
Final Report
March 22, 2026

AA Team 1
Albuquerque Academy

Created by:
Harrison Schiek

Mentors:
Dr. Michael Chandross, Sandia National Laboratories
Mr. Jay Garcia, Albuquerque Academy

Table of Contents

Executive Summary

Problem

Additive Manufacturing (AM) and, more specifically, 3D printing are strongly growing industries with new applications opening in mechanical, biomedical, construction, aerospace, scientific research, and food industries [1,2,3,4,5]. Despite all of this growth, understanding and modelling falls short, usually relying on studies of inference [6] or focusing on Finite Element Analysis (FEA) [7] rather than including the detail of atomistic interactions. One particularly pointed process overlooked in current research is polymer entanglement [8], which is what allows polylactic acid (PLA) to be strong and flexible. Support for and wide usage of PLA is vital due to its unique biodegradability, which prevents huge plastic damage to ecosystems [9].

Materials and Methods

To address this missing consideration of polymer entanglement, atomistic simulations using Large-scale Atomic/Molecular Massively Parallel Simulator (LAMMPS) [10] were conducted to calculate the relaxation time of PLA to approximate the rate at which PLA diffuses and entangles [11]. These simulations utilized data obtained from Ligand Parameter Generator (LigParGen) for small chains [12]. A Python script was written to extend these from 6 to 600-800 monomers. The relaxation time was calculated from an autocorrelation of the end-to-end polymer length, which allowed calculation for the extent of diffusion [13]. To gauge the impact of polymer entanglement on tensile strength, several tensile tests were performed on 3D-printed samples after varying heat treatments informed by the relaxation time.

Verification and Validation

Two verification steps were completed, the first to check agreement with the relationship of molecular weight on relaxation time presented in Thimm et al. [14] and the second to verify accordance with the Williams-Landel-Ferry Equation [15]. Both demonstrated useful trends yet only one with numerical accuracy. A validation test of consensus with experimental relaxation data from Patti et al. [16] for commercially available PLA yielded a significant difference.

Results and Conclusions

Material tensile tests yielded strong results, showing polymer entanglement to have a fairly large impact on tensile strength. While some uncertainty remains, it is likely that, with improved procedures, parts could have as much as 5.8% greater tensile strength.

Problem

Polylactic acid (PLA) presents several key properties that make it crucial to global industry, scientific efforts, and environmental improvement in Additive Manufacture (AM) and Fused Deposition Modeling (FDM). AM promises to revolutionize manufacturing with regard to personalization [17]. Complete design independence between customers could allow entire new industries based on serving specific and individual needs. Similarly, scientific development and experimentation often relies on expensive prototyping and project-specific parts, both of which fall drastically in cost when built using FDM [5]. All of these benefits are crucial as PLA serves as a credible material for wide usage in FDM. Better understanding of PLA and bonding quality will allow PLA to better fit industry needs [18]. The usage of PLA in these areas is essential, as PLA is highly biodegradable and is even manufactured largely from corn processing byproducts [9]. For comparison, it takes a piece of PLA several months to degrade under aerobic conditions [19], while conventional plastics can take up to 450 years [20]. Wider PLA usage in the numerous applications of AM can effectively mitigate the environmental impacts of manufacturing. The question then remains: How can PLA be better understood and supported to be utilized for industry-wide processes?

Current understanding of PLA and other FDM materials lacks a deep and nuanced understanding of the molecular components and their structural interactions. A good portion of FDM procedures are based on inference of observed characteristics and varying processes [6]. This knowledge, while useful for singular improvement, does not allow deeply-informed optimization, which could recommend and successfully implement a variety of improved procedures. Examples include heat treatments, chemical additives, or even printing path or 3D design changes. Furthermore, current research and modeling efforts focus predominantly on Finite Element Analysis (FEA) and coarse-grained Brownian Dynamics [7], which overlooks some of the deep structural nuance of polymer interactions at the atomistic scale. Especially in light of some of the properties that result like biodegradability, atomistic consideration could yield stronger understanding of other properties and insight into process and material optimization. Only after concrete molecular and nanostructural understanding of PLA is achieved can methods really support the full capability of this material. While there are a number of structural and chemical questions which could provide substantial insight, the focus of this project is nanoscale polymer entanglement and its effect on tensile strength. More directly, the aim is to answer the question: “To what extent does polymer entanglement impact the tensile strength of PLA?”

The specific and immediate effect of this question is to inform the use of heat treatments post-manufacture to give more time for diffusion of polymers and formation of entanglements. Among other possible implications for manufacturing, this could allow higher standards of strength for the above uses such as personalized products, prototypes, and experiment-specific parts, improving the industry-wide uptake of PLA as a viable, biodegradable alternative.

Materials and Methods

Overview

A brief overview of the project stages is helpful for deeper understanding of the individual methods and their roles. To begin, LigParGen was utilized to generate parameters for small PLA polymers of 2 to 6 monomers [12]. Then, a Python script was written to edit existing data files to accurately calculate longer polymer parameters and generate approximate structures. These modified input scripts were then used as system inputs for LAMMPS [10], which was utilized to analyze the polymer dynamics. To increase the capability of these simulations, the Simple Linux Utility for Resource Management (Slurm) [21] was used to queue and parallelize LAMMPS to take advantage of available HPC clusters, expanding computing power to hundreds of CPUs over long periods of time. Once these long simulations were completed, a polymer segmental dynamics analysis approach was utilized to determine the relaxation time. This was key to deducing the extent of polymer entanglement in lieu of full, though costly, simulations of polymer melts. Calculating the relaxation time allowed the preparation of 30 material samples with varying degrees of polymer entanglement to thus determine polymer entanglement’s impact on tensile strength. Throughout this process and especially in interpreting and visualizing results, Ovito [22] and Python libraries Matplotlib [23], NumPy [24], SciPy [25], and Pandas [26] were crucial. Access to HPC clusters at the University of New Mexico Center for Advanced Research Computing (CARC) was essential in completing simulations of larger polymers for longer time-scales.

LAMMPS Definitions

To begin, it is important to consider how LAMMPS defines its inputs such that those inputs may be effectively processed to yield the desired simulations. As a helpful background, LAMMPS is a particle simulator designed for practically all lengthscales. Its main function is to carry out many individual interactions on an input particle set in a highly parallelized fashion. These interactions are defined in a system data file. This section is broken into five parts, each one considering the important changes made to system data file inputs.

System data files have 11 important pieces; however, 6 of them do not change as the polymer length is extended. Those sections are definitions for particle type masses, particle pair coefficients, bond coefficients, angle coefficients, dihedral coefficients, and improper coefficients. This is due to the fact that the coefficients defining the relations between the polymer’s atoms do not change since they are the same types of interactions throughout the polymer. These coefficients will play an important role in contextualizing the interactions extended in the other parts. It’s best to first consider the context of extension then to examine each of the sections that need modification in turn. There is also a note at the end of the section concerning the model for pairs.

Extension Context

System parameters for PLA were initially obtained from LigParGen; however, its outputs were limited such that the longest PLA polymer obtainable is 6 monomers long. This is inadequate for realistic simulations, as typical PLA polymers in FDM substrate are in the range of “30,000 - 60,000 g/mol” [27]. This equates to approximately 416 to 833 monomers long, given a molar mass of 72.1 g/mol for each PLA monomer. To generate longer polymers, a Python script was created to define the thousands of atoms and interactions. It was written with 5 main sections for each of the parts that needed modification: atoms, bonds, angles, dihedrals, and improper dihedrals (impropers).

Atoms

Under the ‘full’ specification, LAMMPS very generally defines atoms with an ‘atom type,’ a charge, and a position input. See Figure 1 for a simplified model of a PLA polymer. To add monomers onto the end of the polymer, first the tailing hydrogen is removed then 9 atoms are added. Handling the needed 'atom type' and charge is simple with these additions, as they are replicates of their corresponding atom type and charge in this set order (C1, C2, C3, O1, O2, H1, H2, H3, H4). This order is arbitrary, but it is consistent through the program so as to assure agreement in later assignment of bonds and other properties. Some minute changes are also needed such as changing the type of the final oxygen, as the oxygen in a hydroxide group is functionally different from an oxygen bonded to two carbons. These changes, however, were minute and only affected the ending segments.

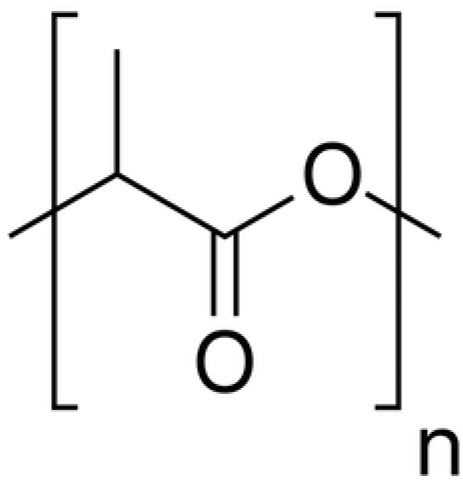

Figure 1 - PLA's repeating structure where n is the number of repeat units in the polymer. The repeating piece has 9 atoms, 3 carbons, 2 oxygens, and 4 hydrogens (not shown, 3 on the methyl group, one on the central carbon on the left) [28].

Atomic position, the final needed piece of the atoms input, is more complicated and was dealt with in two ways. First, since the extension algorithm extends from a PLA polymer with 2 monomers, for the next 4 monomer additions, positions are well known. For these atoms, positions are simply used from the known form. For additions beyond the 6th monomer, the symmetries of the PLA structure served as a basis for position generation. Since PLA adopts a trans-conformational pattern with each monomer (i.e. each monomer is related to the previous one by an approximately 180 degree rotation about the backbone), it was observed that a monomer was approximately a linear transform of the previous second to last monomer, see Figure 2. From this observation, a general offset was determined and added monomers were extended from their respective base monomers in a linear fashion to achieve a polymer of the desired length.

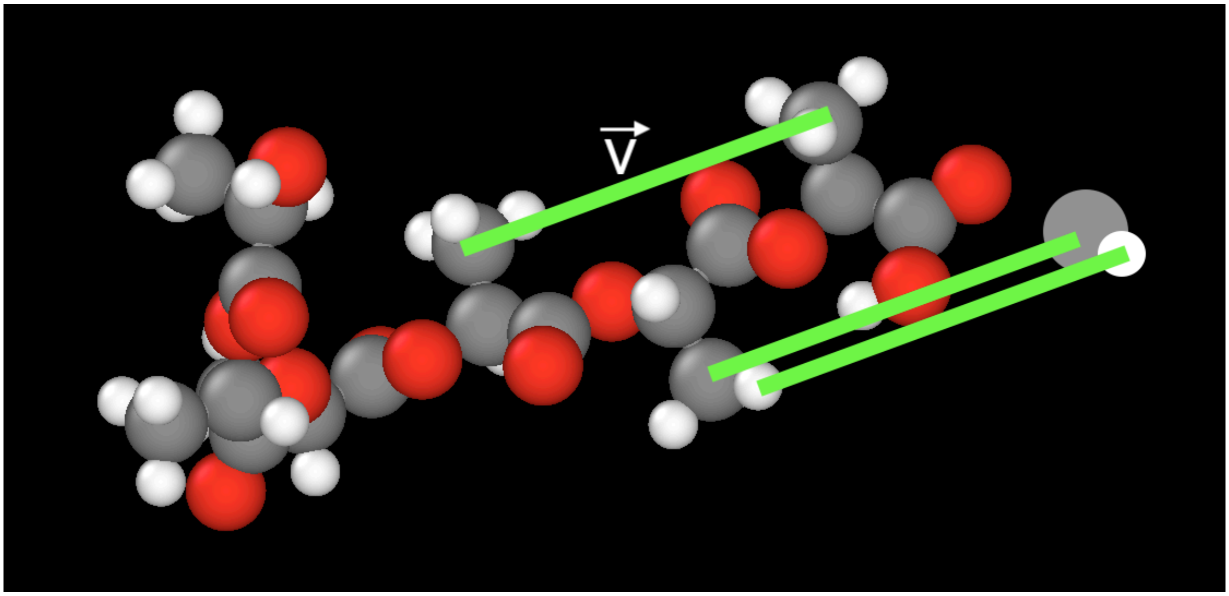

Figure 2 - A PLA polymer with 6 monomers rendered with Ovito. The general offset $\vec{V}$ used to extend is labelled in green, and a sample extended carbon and hydrogen are shown to illustrate usage.

Bonds

LAMMPS defines bonds by a type and a reference to each atom participating. The specific model of bonding used in this investigation was the harmonic model. This essentially approximates the bonds in a given molecule as ideal springs that exert force only along the line of the bond and with magnitude proportional to the change in length, see Figure 3. In the following sections, more nuanced orientation and structure of the PLA polymer are defined with the use of angles, dihedrals, and impropers, which exert force in different ways to specify the manner in which the polymer can move. The governing equation of harmonic interaction is as follows.

$$V = k\left(r - r_0\right)^2 \text{ and thus } F = \frac{dV}{dr} = 2k\left(r - r_0\right), \tag{1}$$

where r is the length of the bond, r_0 is the equilibrium length, k is the spring constant, V is the potential, and F is the force. The constants k and r_0 are defined in the existing bond coefficients section from LigParGen. The type number included in the instantiation of the bond refers to which set of constants to use. Bonds were synthesized for additional monomers in a two part process.

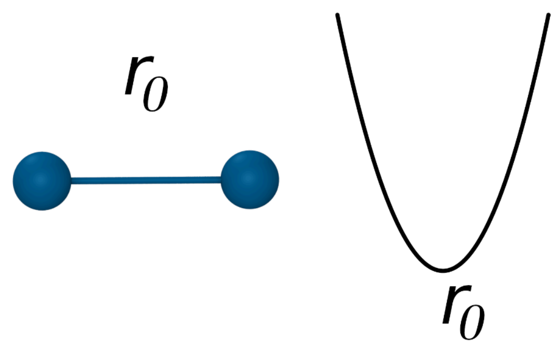

Figure 3 - The harmonic model for bonding. The bond is shown on the left and the used potential (V) is shown on the right [29].

The first part was to identify bonds in the original definition files (of a PLA with 6 monomers) concerning the addition atoms (the C1, C2, … from above) but not the atoms which follow them. This selects not only bonds that interconnect the atoms of the added monomer (intramonomer interactions) but also bonds that connect the monomer to the previous monomer. It is crucial, though, that it does not select the bonds between the added monomer and the atoms that come after (i.e. not including what are essentially 'future' atoms in the context of extension). These interactions are recorded and applied for each monomer added, connecting each one within itself and to the previous monomer such that no interactions are double counted. For each bond identified, the type number and relative indices for each atom were recorded. Once the extension algorithm has finished with all the new monomers and their interactions, a final hydrogen is added and, with it, the one bond to the final oxygen. Think of this like a long fence where each post is a monomer and the fencing in between are the interactions between them. This algorithm makes the fence longer by adding pieces made of a post and the fence before it. This concept will play a crucial role in the algorithms for the remaining interactions (angles, dihedrals, and impropers), and is vital to understanding the addition algorithm especially as the phenomena themselves become increasingly abstract.

Angles

LAMMPS similarly defines angles as a type and the three atoms included in it (with the second atom being the central atom). For this investigation, the harmonic model of angles is used. This model essentially treats the angle as a spring, see Figure 4. The governing equations are very similar to the above, see Equation 2.

$$V = k\left(\theta - \theta_0\right)^2 \text{ and } F = \frac{dV}{d\theta} = 2k\left(\theta - \theta_0\right), \tag{2}$$

with θ being the angle of the bond, θ_0 being the equilibrium angle, k being the spring constant, V being the potential, and F being the force. The constants are once more defined previously by LigParGen and are used unmodified throughout the model. Each angle instantiation has the type number referring to which set of constants to use. For angles, the same general algorithm for extension is employed. Searching the given angles, angles concerning the atoms to be added but not atoms beyond that are recorded with their type number and the relative indices of each of the atoms included.

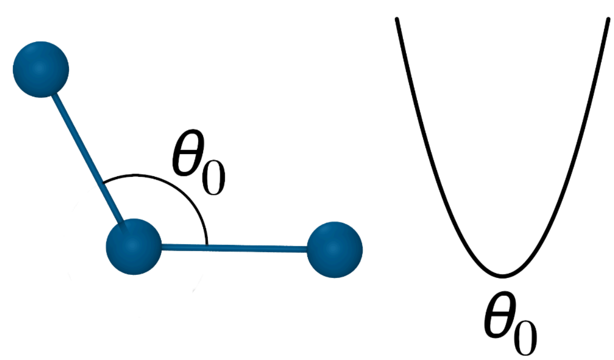

Figure 4 - The harmonic model of angles. The angle is given on the left and the potential is given on the right [29].

Dihedrals

LAMMPS defines a simple dihedral interaction with a type number and four atoms. A dihedral angle is generally defined as the angle deviation of the plane formed by the first 3 atoms and the plane formed by the last three atoms (see Figure 5). It is required that bonding exists between the first and second, the second and third, and the third and fourth atoms. The Optimized Potentials for Liquid Simulations (OPLS) [30] model of dihedrals is used, as they pertain most directly to the melt segmental dynamics of these simulations. OPLS dihedrals are governed by the following equations, see Equation 3.

$$V = \frac{1}{2}K_1[1 + cos(\phi)] + \frac{1}{2}K_2[1 - cos(2\phi)] + \frac{1}{2}K_3[1 + cos(3\phi)] + \frac{1}{2}K_4[1 - cos(4\phi)]$$
$$F = \frac{dV}{d\phi} = \frac{-1}{2}K_1 sin(\phi) + K_2 sin(\phi) - \frac{3}{2}K_3 sin(3\phi) + 2K_4 sin(4\phi), \qquad (3)$$

with K_1 through K_4 being dihedral constants, ϕ being the dihedral angle, V being the potential, and F being the force. These are once more similarly extended to the added monomers. The dihedral constants are taken from the dihedral coefficients section defined by LigParGen and referred to here by type number. With each monomer including its respective dihedrals concerning itself and the previous monomer, this process systematically adds all needed dihedral interactions without double counting.

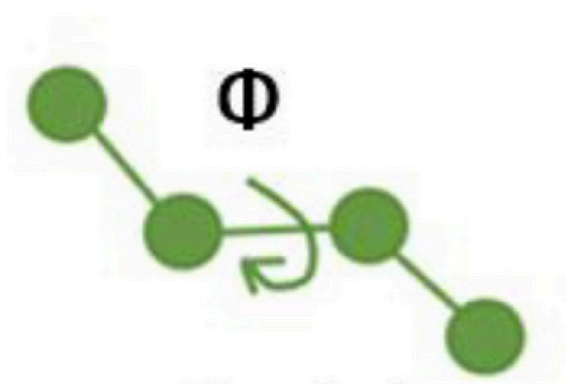

Figure 5 - A dihedral (torsion) angle as defined upon four atoms. Imagine the plane formed by the first three atoms and that formed by the last three atoms, then consider the angle between the two planes [31].

Impropers

Finally, impropers (or improper dihedral angles) complete the needed detail to model PLA. For this project, the Consistent Valence Force Field (or CVFF) [32] model for impropers is used, as it is the standard used by LigParGen. CVFF impropers are defined with a type number and four atoms, which once more define two planes (one with the first three atoms and one with the last three atoms) and are concerned with the angle between them, see Figure 6. This definition, however, does not assume nor require bonding between the second and third and the third and fourth atoms (as is typical in a normal dihedral). It is used instead in cases where the first is bound to each of the other atoms. This model is governed by these more general equations, see Equation 4.

$$V = K[1 + d\cos(n\varphi)] \text{ and } F = \frac{dV}{d\varphi} = -Kdn\sin(n\varphi), \tag{4}$$

where K is the improper dihedral constant, d is either -1 or 1 depending as defined in the coefficient section, n is a positive integer, and φ is the angle of the improper dihedral. Once more, in the same way as above, these interactions are extended monomer by monomer, relating to the last addition, wrapping up with a hydrogen.

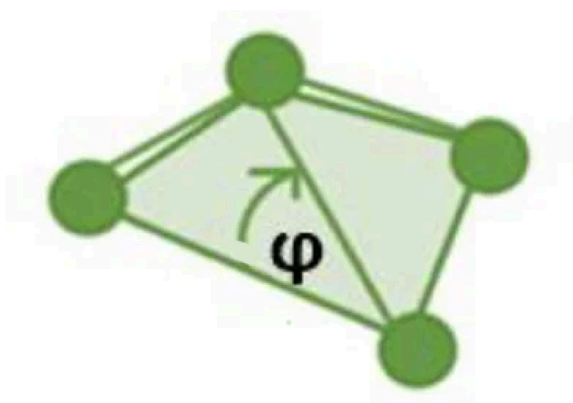

Figure 6 - An improper dihedral angle as defined on 4 atoms. Mentally visualizing the two planes here is difficult; however, if the atom on the far left forms a plane with the two atoms on the right and bottom, and that plane is compared to the plane formed by the three right-most atoms, then the angle φ is defined as the angle between them [31].

Pairs

Lastly, defining the model for pair interactions is important. It's important to note that pair coefficients do not change, and they are attached to 'atom type,' which is already handled by the extension algorithm. Definition of this model, though, is crucial to getting valuable results.

Given the context of the simulation: atoms with pair coefficients and charges, the natural setting would be a Lennard Jones potential with a coulombic addition; however, even LAMMPS simulations run based on verified files from LigParGen diverged when electrostatic interactions were included. Thus, the electrostatic interactions have been neglected, and only Van Der Waals attraction and excluded volume pair interactions (summarized in a Lennard Jones potential) were calculated. The used pair interaction model is a Lennard Jones potential with a cutoff at 9.5 Å, which is typical for atomistic simulations. Its governing equations are as follows, see Equation 5.

$$V = 4\varepsilon\left[\left(\frac{\sigma}{r}\right)^{12} - \left(\frac{\sigma}{r}\right)^{6}\right] \text{ and } F = \frac{dV}{dr} = 4\varepsilon\left[\frac{-12\sigma^{12}}{r^{13}} + \frac{6\sigma^{6}}{r^{7}}\right], \tag{5}$$

where ε is the 'depth' of the potential well (-ε being the lowest energy state of the potential), σ is distance at which the energy of the interaction is 0, and r is the distance between the atoms. These coefficients are specified and referred to from the pair coefficients generated by LigParGen.

To conclude, among all 6 of these types of interactions, for a polymer with 800 monomers, there are some 47,000 interactions with around 250,000 modeling parameters to accurately simulate the polymer. Even beginning to model a singular PLA molecule entails a great deal of complexity.

LAMMPS Setup

Once the initial structure of the PLA polymer has been defined, the next major step is setting up and running the simulations to calculate the relaxation time. This usage is concerned with the atomistic scale, and there are two major settings that contextualize the usage and initialize the properties needed.

Units and Atom Model

First, the units are defined as 'real.' That is, units of distance are Angstroms (Å), units of time are femtoseconds (fs), units of mass are grams per mole (g/mol), units of energy are kilocalories per mole (kcal/mol), and units of temperature are degrees Kelvin (^{o}K). Additionally, the atom model is set to full. That is, each atom has charge, location (x, y, z), velocity (x, y, z), atom type, mass, and a molecule number. Atom type refers to the mass and pair coefficients defined previously. Molecule number simply denotes the grouping of atoms.

Ensemble

Lastly, understanding and manipulating statistical ensembles as theoretical bases for these simulations is necessary for accurate representation. There are numerous ensembles that are relevant for molecular dynamics: microcanonical, canonical, grand canonical, etc. and each are characterized by the properties they hold constant. The ensemble most used in this project for these simulations is the microcanonical ensemble, which holds particle number, energy, and volume constant, while allowing temperature, pressure, and chemical potential to vary. This ensemble is analogous to if the simulation were done in a container with fixed volume and no interactions with the outside, see Figure 7. The other ensemble used in this project is the Canonical or NVT ensemble, which holds particle number, volume, and temperature constant, while allowing energy, pressure, and chemical potential to vary. It is analogous to a similar situation but now allowing temperature flow (Figure 7). Another ensemble type which is planned to be used in further extensions of this investigation is the Gibbs ensemble or the isobaric-isothermal ensemble, which holds pressure, particle number, and temperature constant by allowing volume, energy, and chemical potential to vary. This would be useful in condensing many polymers into a full material, which is necessary for more realistic polymer melts and for further material testing..

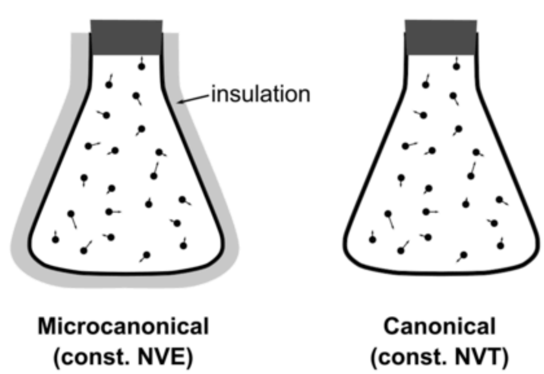

Figure 7 - A general model of microcanonical and canonical ensembles [33].

LAMMPS Simulations

Once these parameters have been defined, it is possible to begin simulations. In these simulations only one polymer molecule was simulated, and it was simulated in isolation without any background solvent. There are two major steps to achieving an accurate amorphous polymer simulation. Then, when analyzing the data, using an autocorrelation allows for calculation of the relaxation time. Ovito was used to visualize the outputs of these simulations to diagnose errors and gauge progress. A Python script operating on separate outputs was utilized to complete the autocorrelation.

Collapse Simulation

The first simulation step is a rapid collapse where the initial linear polymer is allowed to relax into the natural configuration of a random coil. This step erases the artificial initial condition of a completely elongated polymer to ensure realistic progression for later calculations. It is easy to confuse the time it takes to relax from this linear state with the relaxation time; however, they are distinct. See Figure 8.

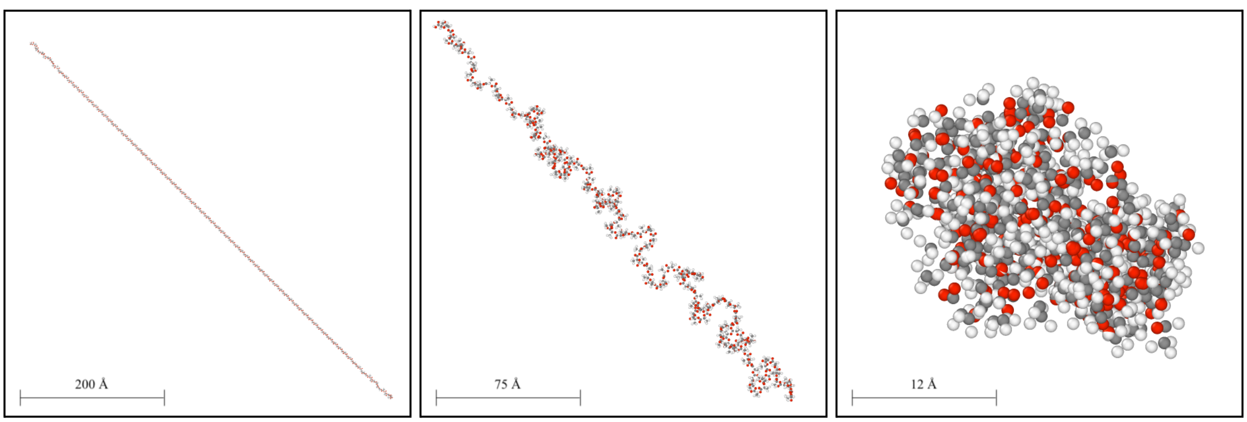

Figure 8 - The 1st stage of polymer simulations, a collapse from unnatural strain to a natural configuration. A PLA polymer with 150 monomers is simulated. The images shown (left to right) are 0 ps, 50 ps, and 82 ps. They are progressively more zoomed in to provide a better view of the polymer. Bonds are not shown. Atomic radii are not to scale. These images were rendered with Ovito.

Unsurprisingly, relaxing from a linear state to a ball releases a lot of energy because the entropy of the system rises immensely, progressing from perfectly linear to random coil. Temperature rises immensely, see Figure 9. Additionally, resulting polymer balls typically retain some residual momentum from the collapse which would affect later determination of relaxation time. Since relaxation time is dependent on temperature, it is important that this natural configuration is restarted at relevant temperatures.

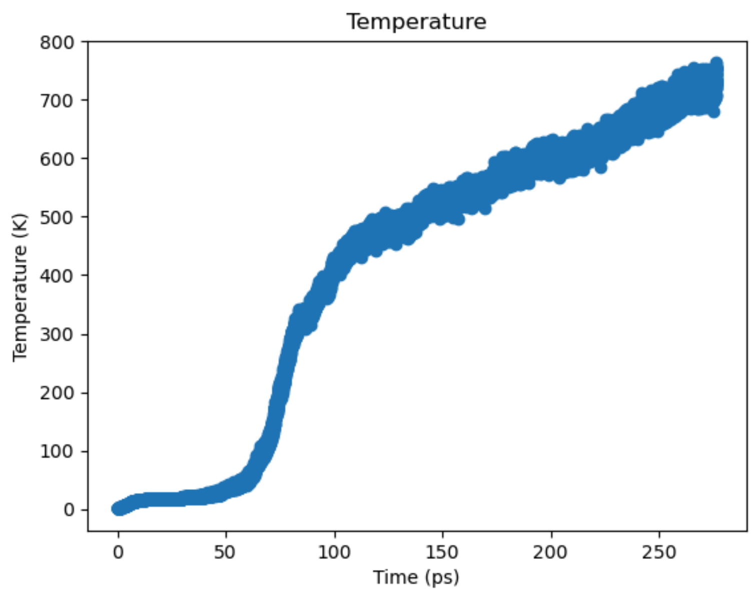

Figure 9 - The temperature of the above example collapse simulation (Figure 8). Note the final temperature of around 700ºK. Also note the corresponding temperatures for the above snapshots: 0 ps, 50 ps, and 82 ps. Simulation after 82 ps serves to convert residual potential energy into kinetic energy which may be easily reset to preserve accuracy in natural configuration. This simulation took nearly 30 million time steps.

To reset the temperature and momentum of the polymer once collapsed to a random coil, a Python script was written to import the location data of the atoms in this simulation into a new system file so as to start the simulation with no preexisting momentum at a specified temperature with only minimal traces of the previous simulation. This first type of simulation was often repeated for long polymers like PLA with 800 monomers since the energy released from partial collapse was enough to prevent further progression to random coil.

Relaxation Simulation and Data Analysis

Once fully equilibrated in a random coil configuration, the polymer system was simulated at a variety of temperatures including typical 3D printing temperatures (488ºK or 215ºC) to gain an effective understanding of PLA's relaxation time.

In these second stage simulations, the end-to-end length *R* was calculated from the location of the first and last monomers. This gives a valuable sense for the movement of the polymer, which can be used to calculate the relaxation time. In this project, it is assumed that there is only one relaxation mode of the polymer. The source of the following conclusion is a paper which investigates many relaxation modes of complex proteins in a biomolecular context; however, in these simulations a singular mode is more likely. It is important to note that this assumption fit very well on simulation data; thus, the dynamics are well captured by a single relaxation mode. The following modified conclusion from Mitsutake et al. 2017 [34] serves as a valuable means with which to consider PLA's relaxation and thus diffusion.

The relaxation mode X_p satisfies

$$\langle X_p(t) X_p(0)\rangle = \delta_{p,p} e^{-\lambda_p t}, \tag{6}$$

where $\langle A(t), A(0)\rangle$ denotes the autocorrelation between *A* at time *t* and *A* at time 0, λ_p is the relaxation rate, and $\delta_{p,p}$ is a constant associated with the mode. The relaxation time, or the inverse of the rate, $\frac{1}{\lambda_p}$, is valuable in this investigation, as the relaxation time is roughly approximated by the time required for a polymer to travel its own length while suspended in polymer melt [11]. The autocorrelation of a series is calculated as the correlation of that series to itself with some shift called lag. It's important to note that for a data set that is some length *l*, the autocorrelation has the strongest meaning only up to $\frac{l}{10}$, and so many of the following simulations are 10 times as long as the maximum lag shown. Take the example of a PLA polymer with 400 monomers at approximately 550ºK, see Figure 10 for its autocorrelation.

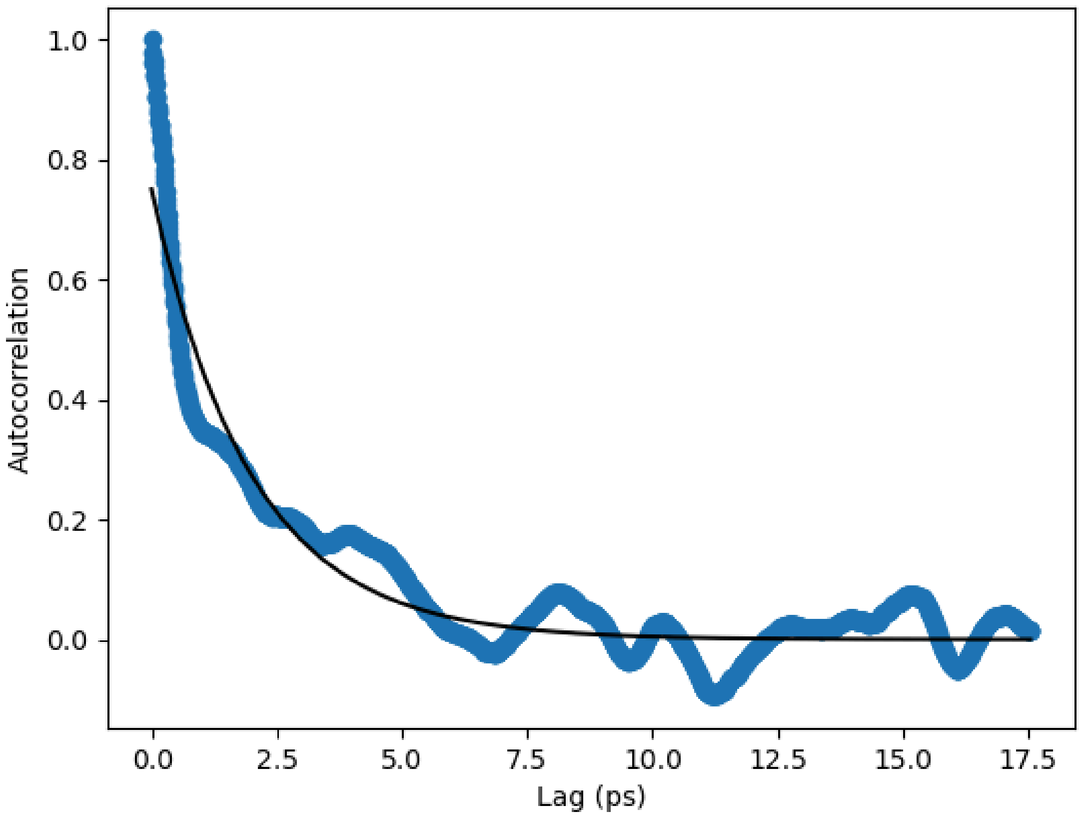

Figure 10 - The example autocorrelation of the end to end length *R* of a PLA polymer with 400 monomers at 550ºK is shown in blue. The exponential fit of the data is shown in black. This fit achieved an R^2 of 0.90, suggesting a reasonably strong agreement. It was rendered and calculated using a script written for data analysis. The full simulation for this data was 175 ps long.

From this fit, the relaxation time can be calculated according to Equation 6. The specific fit parameters of the above graph are $\delta_{p,p} = 0.750$ and $\lambda_p = 0.504\, ps^{-1}$. Thus, the relaxation time of a PLA polymer with 400 monomers at 550ºK $\tau = \frac{1}{\lambda_p} = 1.98\, ps$. It's important to note that the good fit achieved confirms that the dynamics are well captured by a single relaxation mode model.

Slurm High Performance Computing

All of these simulations take a large amount of computing power and would not have been possible without the incredible support of UNM's Center for Advanced Research

Computing. Many of these simulations took 12 hours or more on as many as 128 CPUs to run many millions of steps to simulate some hundreds of picoseconds, making independent computing simply not feasible. Thankfully, LAMMPS scales exceptionally well; however, Slurm was still crucial in running the necessary jobs on the available High Performance Computing (HPC) architecture. All of these simulations were run via slurm's batch scheduler using the sbatch command and input bash files. Through this infrastructure, allocation and parallelization hierarchy could be specified. One interesting issue that surfaced in this area was that once run via the Slurm system, LAMMPS would not parallelize internally given more computational power per task. e.g. a LAMMPS instance when divided into two tasks and given 16 CPUs per task would only utilize two CPUs in total (one per instantiation). The result was poor efficiency until allowing Slurm to control all parallelization; i.e. dividing the task down to one CPU per LAMMPS instance (task).

Material Tensile Test

Last, to gain a concrete conclusion about the impact of PLA polymer entanglement on tensile strength, several ultimate tensile strength tests were completed to measure its impact. These tests consisted of a simple 'dog bone' tensile test piece (see Figure 11), which was 3D printed with 100% infill and varying infill angle (0º, 45º, and 90º) in a horizontal orientation (Figure 12). The distinction in tensile strength resulting from varying infill angle has previously been established in several studies [36,8]. With the help of a Louisware digital caliper, the cross sectional area was calculated as $1.33\ mm \cdot 3.75\ mm = 4.99\ mm^2$. The pieces were 3D printed at 215ºC nozzle temperature and 50ºC bed temperature, using Monoprice's PLA Plus+ and the MP Voxel 3D Printer.

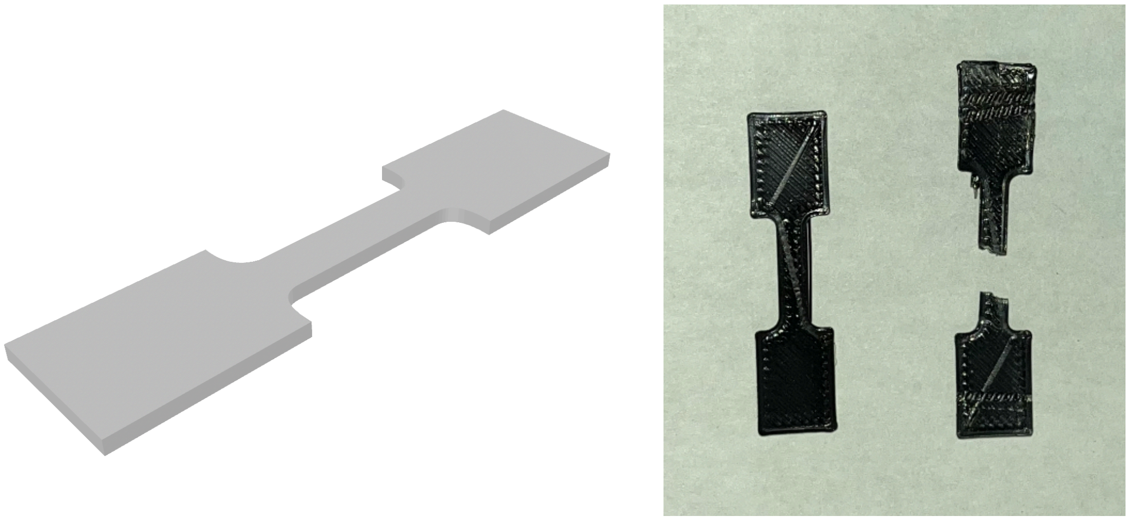

Figure 11 - The ‘dog bone’ testing model used in this project (left) [37]. It was scaled and printed, then subjected to heat treatment and tensile testing. Two ‘dog bones’ one before testing, one after testing shown on the right. Note the 45º infill in the diagonal lines evident on the printed models. The pieces are 8 mm wide, 37 mm long, and 1.33 mm thick.

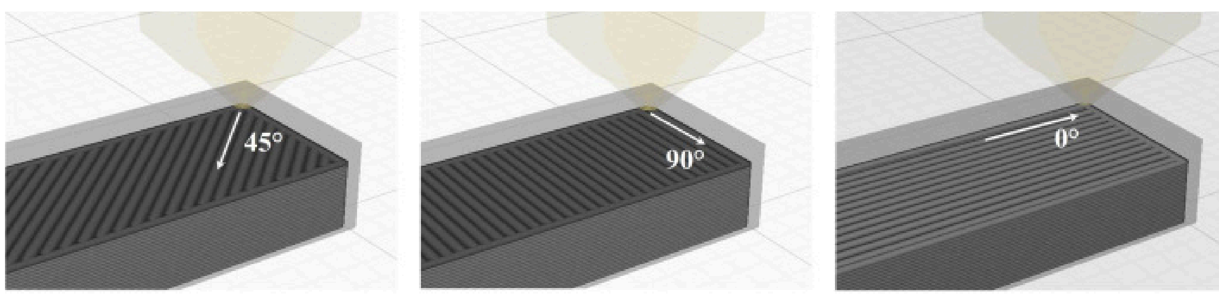

Figure 12 - The three orientations of infill used in this project [8]. Infill orientation has been previously noted in various papers to have a significant impact on the tensile strength of resulting test pieces. It is important to note that, given the size of the tensile tests printed, about half was outline material, which is always in the direction of the pull, thereby reducing the orientation differences observed in this study.

The samples were then randomly subjected to one of two heat treatments: control (stored at room temperature), and full (117ºC for 5 minutes). The calculations leading to this time will be discussed in the Results and Discussion section. The full treatment was achieved by heating a cast iron pan on the stove until fully heated to 117ºC, turning off the heat, placing the samples inside with tin foil coverings, and wrapping it in a towel to maintain temperature. After treatments, the test pieces were held with a clamp to a secure point on a table and with another clamp to a bucket to which a 10 lb weight and sand were added until the sample failed, see Figure 13. The weight that caused failure was recorded. It is assumed that this weight is approximately the maximum force that the sample can hold, given weight is added gradually. The sand was very easy to add in this way, since it could be slowly poured. This weight (force) was then divided by the cross sectional area to calculate ultimate tensile strength (or maximum stress endured), see Figure 14. It is assumed that the cross sectional area is constant for all pieces, as their shapes are all effectively the same. Time from print or treatment to test was kept approximately equal to reduce skew caused by aging. Five pieces were tested for each category for a total of 30 tests.

Figure 13 - Tensile testing setup including the bucket, the 10 lb weight, the sand, the sample (black with red arrow), and the two clamps, one to the table (red) and one to the bucket (gray). Note the gradual addition of sand to slowly approach the ultimate tensile strength of the sample.

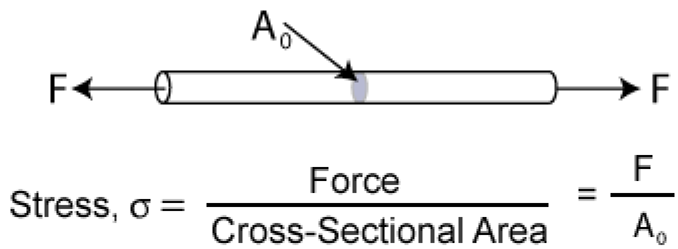

Figure 14 - A situation analogous to the tensile tests used to calculate the stress [38].

Using this procedure, the tensile strength of pieces with differing degrees of polymer entanglement was measured to test the extent to which that entanglement impacts tensile strength. While this setup is not highly precise, it serves as a valuable starting point to make conclusions about polymer entanglement.

To summarize, the initial editing and reformatting of the PLA data files from LigParGen, the setting up the various parameters and specifications of LAMMPS, the first and second stage simulations on UNM HPC clusters, the data analysis, and the experimental material testing all served to accurately simulate and methodically investigate PLA and its polymer entanglement.

Verification and Validation of Simulations

Verification

To determine the effectiveness and accuracy of the simulations, two major verification steps were carried out. The first checks agreement with the molecular-weight to relaxation time relationship presented by Thimm et al. [14]. The second confirms the temperature shift of the relaxation times with the Williams-Landel-Ferry (WLF) equation [15].

Beginning with the first, it is important to consider the four general lengths investigated: 150, 400, 600, and 800 monomers. Those polymers have molecular weights of around 10,800, 28,800, 43,200, and 57,700 g/mol respectively. It is important to note that all of these polymers exceed the critical molecular weight (sometimes referred to as the entanglement molecular weight), which indicates that their dynamics are not in the Rouse regime but rather in the Reptation regime. For context, the Rouse regime is a state of polymer melts where brownian motion and diffusion dominate. That is, the individual polymers do relatively little to hinder the others' mobility [11]. On the other hand, the Reptation regime is characterized by large hindrances on polymer movement caused by entanglements within the polymer and with other polymers [11]. The specific value for the critical molecular weight used here is 8,700 g/mol as referenced in Dorgan et al. [39]. It's important to note that, despite there being only one polymer simulated at a time, the dynamics are still in the Reptation domain because the polymer does in fact experience friction and entanglement with itself. In the future though, simulating a full melt will likely prove much more accurate. This is important in the parsing of the formula presented in Thimm et al., see Equation 7.

$$\tau\,(m) = km^{\beta}, \tag{7}$$

with $\tau(m)$ denoting relaxation time as a function of normalized molecular weight, m being the normalized molecular weight, and k and β being constants; however, it's noted that, in line with other viscoelastic properties with similar relations, β is around 1 for short polymers (with molecular weight less than the critical molecular weight) and β is around 3.4 for long polymers (with molecular weight greater than the critical molecular weight) [11,39].

Using the data gathered from these four examples at 550ºK, the following four autocorrelation curves result, see Figure 15. This high temperature was used to calculate relaxation time of these long polymers without needing immense timescales.

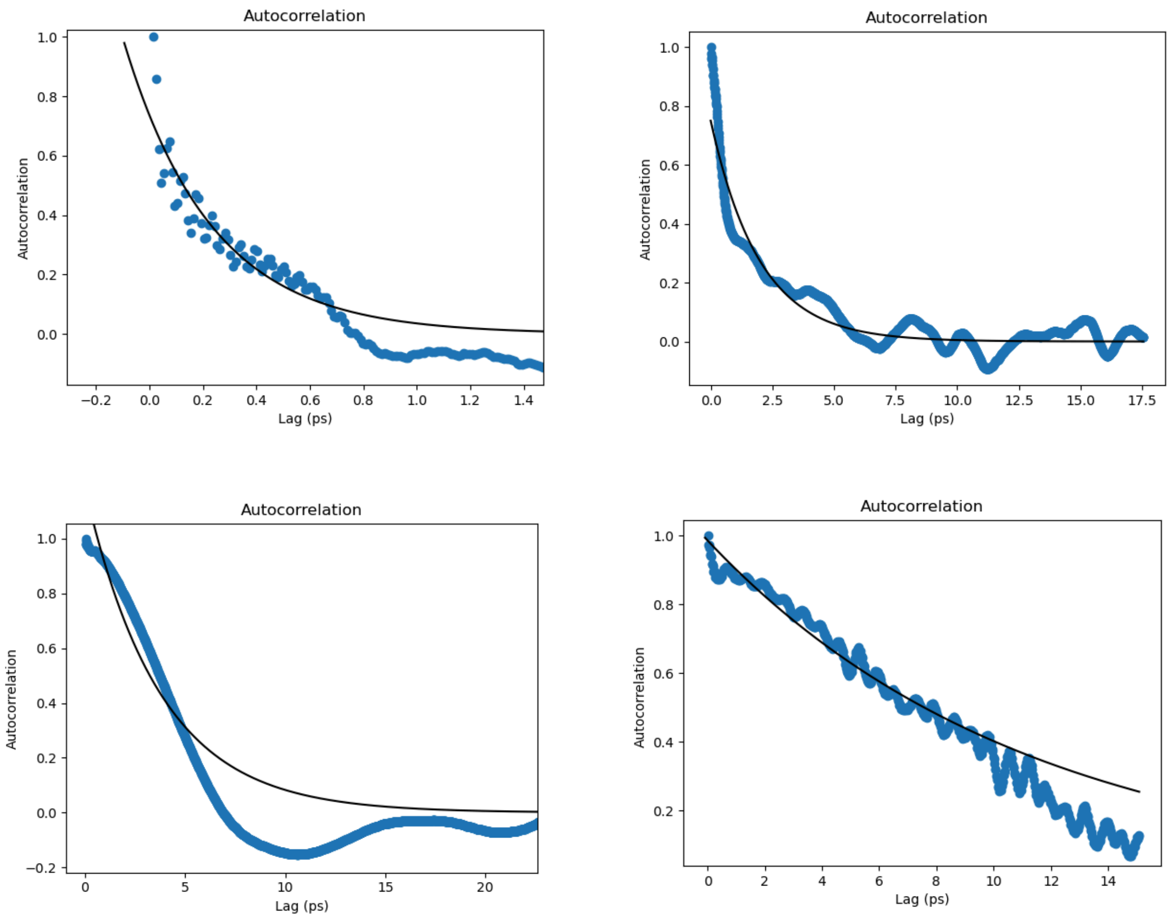

Figure 15 - Autocorrelations for tests of PLA with 150 monomers (top left), 400 monomers (top right), 600 monomers (bottom left), and 800 monomers (bottom right). Note also that the assumption of only one mode of relaxation may be less accurate for PLA with 800 monomers, given the evident noise (bottom right).

The parameters for the fits of the relaxation rates are as follows for 150, 400, 600, and 800 monomers, respectively: 3.01 ps^{-1}, 0.504 ps^{-1}, 0.262 ps^{-1}, and 0.0894 ps^{-1}. These rates, when converted to relaxation times result in the following: 0.332 ps, 1.98 ps, 3.82 ps, and 11.2 ps. When fit to Equation 7, they yield a β fit parameter of 3.24, which is within 5% of the ideal value of 3.4. The R^2 was .985, confirming the observed accuracy, see Figure 16. This means that the dynamics worked well to produce accurate numerical results, and, observing the plots of Figure 15, the simulations consistently produced data that fit quite well to the theoretical ideals.

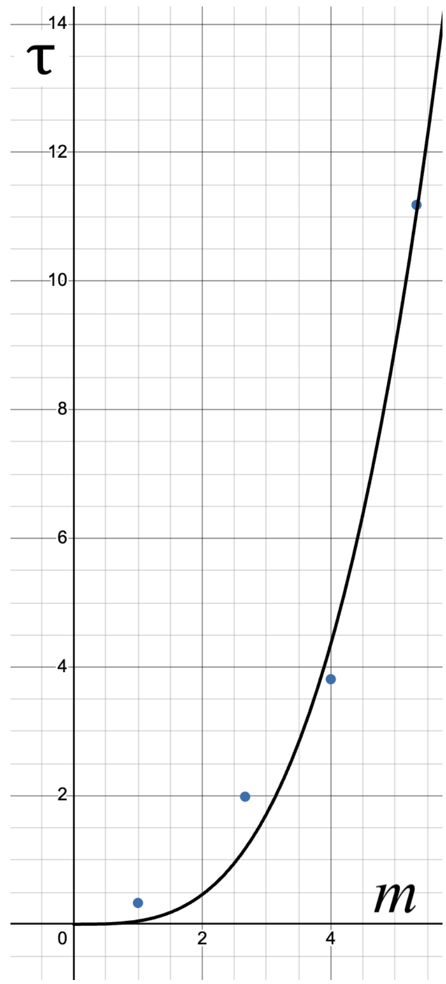

Figure 16 - The fit of Equation 7 to the simulated relaxation times. τ is in units ps. *m*, the normalized molecular weight, is unitless. The fit parameters are $k = 4.89 \cdot 10^{-2}$ ps and $\beta = 3.24$.

Moving to the second verification step, the WLF equation is used to assure proper capture of temperature dependence in the relaxation time. It applies generally to all amorphous polymers. Amorphous is defined as a flexible polymer as opposed to a crystalline or semicrystalline polymer. The WLF equation is as follows (Equation 8) [15].

$$log_{10}(\alpha_T) = -\frac{C_1(T-T_s)}{C_2+T-T_s}, \tag{8}$$

with α_τ denotting the relaxation time shift factor or the ratio of relaxation times at temperatures T and T_s, respectively, C_1 and C_2 being empirical constants, $C_1 = 17.44$ and $C_2 = 51.6$ K [40], and log_{10} being the common log (base 10). Typically T_s is set to the glass transition temperature, which is between 63.0ºC and 63.8ºC for commercially available PLA [41]. To check against this equation, the examples of PLA with 150 monomers at temperatures of 375ºK, 415ºK, and 488ºK were used. Only PLA with 150 monomers was used given long compute times for others and the need to conserve resources. The shift factor was calculated as follows, see Equations 9, 10, and 11.

$$log\left(\alpha_{375^oK}\right) = \frac{17.44\left(375^oK - 336.55^oK\right)}{51.6^oK + 375^oK - 336.55^oK} = 7.45 \text{ thus, } \alpha_{375^oK} = 2.80 \cdot 10^{7} \quad (9)$$

$$log\left(\alpha_{415^oK}\right) = \frac{17.44\left(415^oK - 336.55^oK\right)}{51.6^oK + 415^oK - 336.55^oK} = 10.52 \text{ thus, } \alpha_{415^oK} = 3.31 \cdot 10^{10} \quad (10)$$

$$log\left(\alpha_{488^oK}\right) = \frac{17.44\left(488^oK - 336.55^oK\right)}{51.6^oK + 488^oK - 336.55^oK} = 13.01 \text{ thus, } \alpha_{488^oK} = 1.02 \cdot 10^{13} \quad (11)$$

Thus, the difference in adjacent data points should be around 3 orders of magnitude. Recall the definition of the shift factor as the ratio between the relaxation time at some temperature T and the relaxation time at the glass transition temperature T_g.With that definition, the general statement may be made using substitution and simplification, see Equation 12.

$$\frac{\alpha_{T_1}}{\alpha_{T_2}} = \left(\frac{\tau\left(T_1\right)}{\tau\left(T_g\right)}\right) \cdot \left(\frac{\tau\left(T_2\right)}{\tau\left(T_g\right)}\right)^{-1} = \frac{\tau\left(T_1\right)}{\tau\left(T_2\right)} \quad (12)$$

Thus, the ratio of relaxation times for T_1 = 415ºK and T_2 = 488ºK will be equal to the ratio of the shift factors α_{415^oK} and α_{488^oK}, which is $3.25 \cdot 10^{3}$. Comparing this to the observed change, it may be seen that there is some consistent deviation but the general behavior is in line with the WLF equation, see Figure 17.

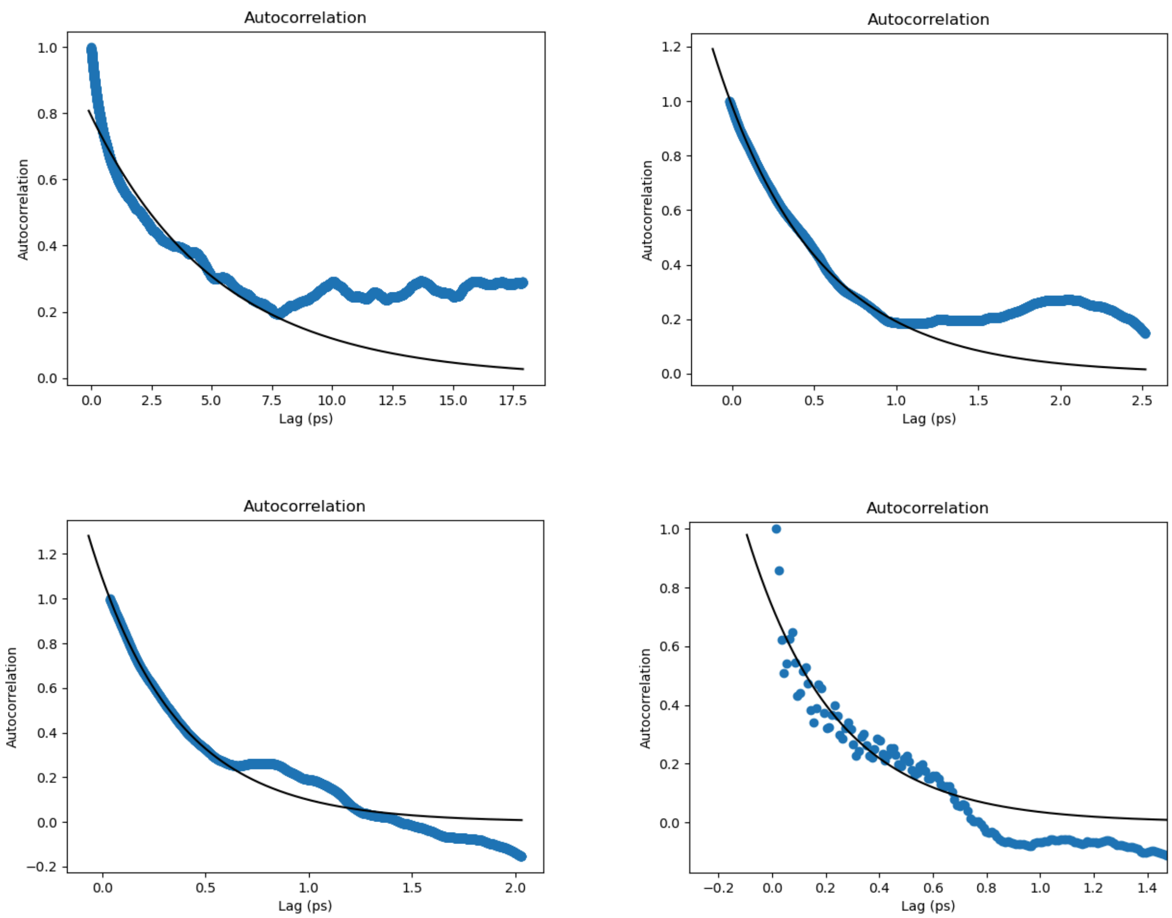

Figure 17 - The autocorrelations of PLA with 150 monomers at 375ºK, 415ºK, 488ºK, and 550ºK. Although 550ºK's shift has not been calculated, it is a piece of data that contextualizes some of the inaccuracies observed here.

The relaxation rates for the PLA with 150 monomers at 375ºK, 415ºK, and 488ºK, respectively are 0.189 ps^{-1}, 1.656 ps^{-1}, and 2.397 ps^{-1}, resulting in relaxation times of 5. 29 ps, 0. 604 ps, and 0. 417 ps. As seen, there was some agreement in the shifting, as the simulated values did trend in the right direction, with rates that increase with temperature (see increasing slope/decreasing timescale as temperature increases in Figure 17). This aligns with the above shift factors, in that the relaxation times did decrease with increasing temperature. The magnitude of change, however, was not consistent with the theoretical ideal. The WLF equation predicts a difference of 10^3, but the simulated results only deviated by 10^1 at most. With the additional context of the simulated relaxation time of PLA at 550ºK (Figure 17 bottom right), it seems the shift damps with increased temperature, suggesting an instability in the simulated structure. The structure was probably able to change conformationally resulting in an enduring shift in its properties. It is likely that this conformational change was the PLA becoming smaller and more tightly wound, and thus being less mobile. Comparing average end-to-end polymer length between these simulations, the data slightly supports this hypothesis (see Figure 18). It is important to note that this shift is probably due to the lack of electrostatic forces, as these provide a crucial repulsive force. These could have prevented the observed changes by not allowing the slight tightening of the coil. It could also be that 150 monomers is effectively too short in the altered background of the simulations, producing noisy data.

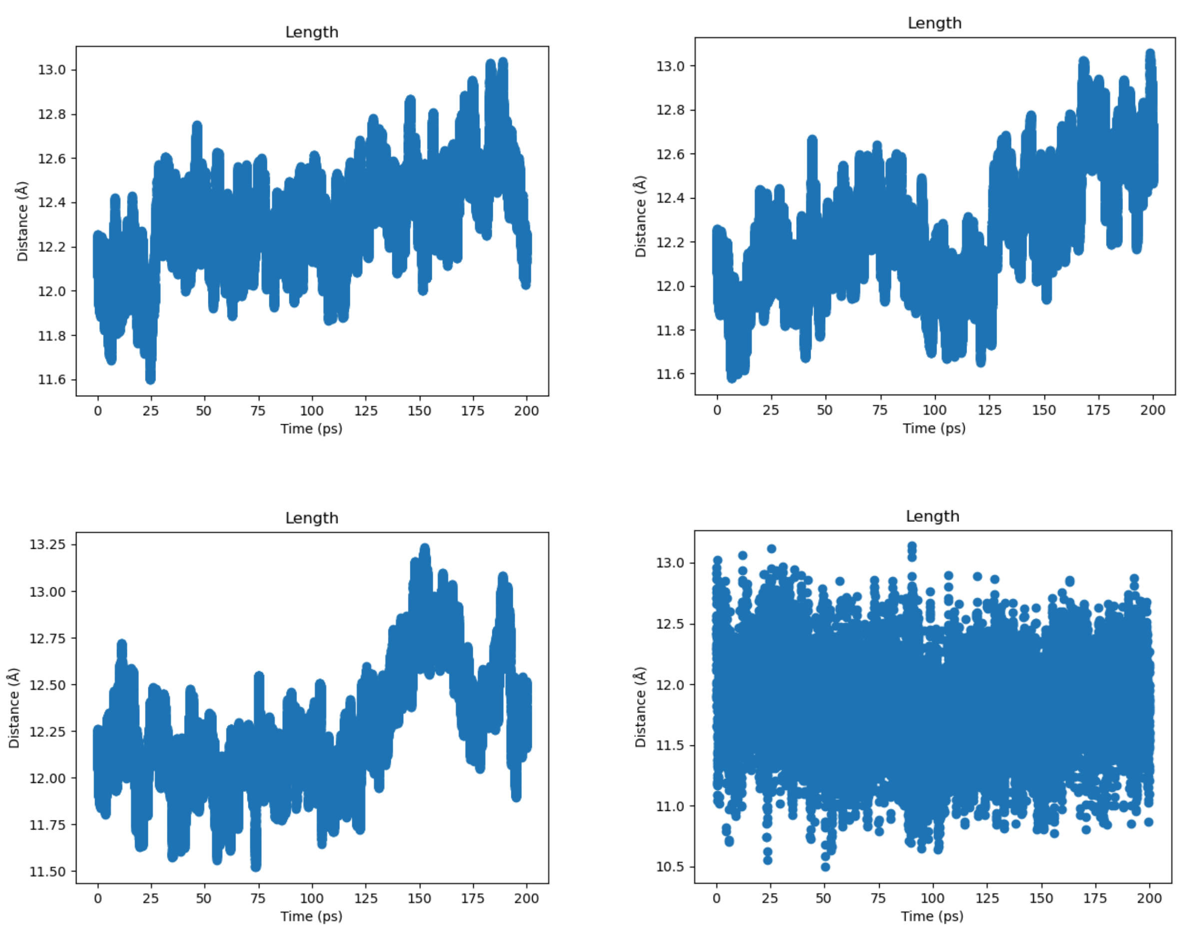

Figure 18 - The length per time graphs for PLA with 150 monomers at 375ºK (top left), 415ºK (top right), 488ºK (bottom left), and 550ºK (bottom right). Note the slight downward trend in their average length. Also note that there should be the opposite trend due to thermal expansion.

Through these two verification scenarios, it has been shown that the simulations were moderately accurate to the end of determining the relaxation time. They present many similar trends and consistently show ideal features in their autocorrelations; however, it is evident that there is some discrepancy between the theoretical ideals and the simulated results. This means that, while the numerical results of the simulations may be slightly skewed, it is likely that the behavior and substance of the model does correctly simulate the polymer. The high alignment of simulation autocorrelation to the exponential model and the accuracy of molecular weight scaling confirms the correct fundamental behavior and data interpretation; it is only a matter of improving the background and interactions to attain more accurate results.

Validation

To add context surrounding the efficacy of these simulations, it is also important to compare the simulated results to those observed in an experimental context. The results of Patti et al., an experimental study of commercially available PLA 3D printing filament, measured the relaxation time as 0.243 seconds and 0.295 seconds for two suppliers at 170ºC (443ºK) [16]. This value shall be compared to the result of the above simulation of PLA with 800 monomers at 550ºK: 11.2 ps. Using the average of the two results from Patti et al. [16] and converting by temperature using the method above, the following two shift factors were found, and the conversion computed, see Equations 13 and 14.

$$log\left(\alpha_{443^oK}\right) = \frac{17.44\left(443^oK - 336.55^oK\right)}{51.6^oK + 443^oK - 336.55^oK} = 11.75 \text{ thus, } \alpha_{443^oK} = 5.57 \cdot 10^{11} \quad (13)$$

$$log\left(\alpha_{550^oK}\right) = \frac{17.44\left(550^oK - 336.55^oK\right)}{51.6^oK + 550^oK - 336.55^oK} = 14.04 \text{ thus, } \alpha_{550^oK} = 1.11 \cdot 10^{14} \quad (14)$$

This means that to convert from relaxation time at 550ºK to 443ºK, the simulated result of 11.2 ps must be multiplied by $\frac{\alpha_{550^oK}}{\alpha_{443^oK}}$ or $1.99 \cdot 10^{2}$. Thus the simulated relaxation time converted to 443ºK is 2.23 ns compared to 0.27 s. Understandably, this value differs from the experimental value by quite a few orders of magnitude.

It is understandable as the assumptions made for computational feasibility can account for this difference fairly well. First, the lack of realistic background is likely a contributing factor. Especially when it comes to relaxation time, having the real setting, a polymer melt, for the simulation is important, as friction and blocking from neighbors are very important factors in determining a relaxation time. Without friction with a background of other polymers or tangling with neighbors, relaxation happens faster. Additionally, the lack of electrostatic interactions could contribute as well, as these forces likely would provide a force to restrict movement and thereby slow the relaxation time. Another potential cause could be the lack of particle fillers and chemical additives (as are present in commercial PLA) that could change relaxation times.

Through this validation check, it may be more clearly understood that current modelling parameters solve the useful, though adjacent, problem of PLA relaxation in isolation without electrostatic interactions. It is perhaps not surprising that they do not accurately reproduce all experimental numbers, but rather, demonstrate the commonality of mechanism and trend across problems. There was also still a notable level of accuracy achieved in the scaling with molecular weight, showing the successful dynamics already achieved. This model serves as an excellent basis for further refinement and optimization for the modeling of PLA.

Results and Discussion

To determine the true impact of polymer entanglement on tensile strength, the above tests were performed on the 'dog bone' tensile test pieces. The test pieces themselves were printed with various infill orientations to test the difference between homogenous PLA and bonded interfaces, as shown in Figure 12. The experimental results of Patti et al. [16] for PLA relaxation time were used, as they were more relevant to the PLA melt present in the 3D printing of the 'dog bone' tensile tests used.

It is estimated that when coming into contact with the PLA on the printer plate, the hot (215ºC) PLA very rapidly cools to ~130ºC (the average of 215 and 50) on contact with the 50ºC PLA on the plate. It then cools reasonably quickly to 50ºC. Given Equation 8, the relaxation time as a function of temperature may be given as the following (inserting the known values of C_1, C_2, and T_g, and using T_2 = 170ºC and $\tau(T_2)$ = 0.27 seconds as a base), see Equation 14.

$$\tau(T) = 10^{\frac{C_1(T_2 - T_g)}{C_2 + T_2 - T_g} - \frac{C_1(T - T_g)}{C_2 + T - T_g}} \cdot \tau(T_2) = 10^{11.75 - \frac{17.44(T - 336.55^oK)}{T - 284.95^oK}} \cdot 0.27s \tag{14}$$

This equation comes from the observation that the ratios described in Equation 8 may be used together to gain a more general formula for relaxation time, recall Equation 12. Thus, it follows that for some general *T* and some base T_2,

$$\tau(T) = \frac{\alpha_T}{\alpha_{T_2}} \cdot \tau(T_2) \quad \text{since} \quad \frac{\alpha_T}{\alpha_{T_2}} \cdot \tau(T_2) = \frac{\tau(T)}{\tau(T_2)} \cdot \tau(T_2) = \tau(T) \tag{15}$$

To make simple bounds on the extent to which PLA relaxes in the 3D printing process, consider two boundary cases: the PLA remains at 130ºC throughout the print (lower bound), and the PLA instantaneously cools to 50ºC (upper bound). Converting the above time to a rate and considering a print time *t*, the following boundary relaxation extents result, see Equations 16 and 17.

$$\frac{t}{\tau(130^oC)} = \frac{t}{10^{11.75-9.83} \cdot 0.27s} = t \cdot 4.46 \cdot 10^{-2} s^{-1} \tag{16}$$

$$\frac{t}{\tau(50^oC)} = \frac{t}{10^{11.75+6.12} \cdot 0.27s} = t \cdot 4.96 \cdot 10^{-18} s^{-1} \tag{17}$$

Converting those into print times until complete relaxation, the lower bound needs a print time of 22.44 seconds to reach full relaxation, and the upper bound needs $6.39 \cdot 10^9$ years. Evidently there is uncertainty in how much relaxation is occurring in the print, as the lower bound includes most prints. It is likely the actual temperature tends more towards the upper bound as the amount of convection cooling and the relatively large mass of the existing print aid heat transfer out of the added material as opposed to the small amount of existing heat from when it is deposited. With all of this in mind, it is assumed that for the tensile test pieces used, the material has only experienced some small amount of relaxation.

These results are also very important when considering relevant papers on similar treatments. Take Bertocco et al. [8], which is concerned with infill direction and heat treatments after 3D printing. They find that infill direction has a strong impact on tensile strength with more alignment leading to higher ultimate stress measures. They also find heat treatments at -15°C and 50°C for long periods of time both have a negative impact on the tensile strength. Given these calculations, it is likely those treatments had little impact on polymer diffusion and entanglement, as at those temperatures, no relaxation is expected to occur. Specifically, at 50°C, relaxation would take millenia (Equation 16).

With these previous results and these new calculations in mind, the heat treatments for this project are ‘control’: room temperature storage, and ‘full’: (117°C for 5 minutes) for an overshoot of relaxation time. An overshoot is used to reduce possible error in the heat treatment, such that even if some of the sample is only heated to a lower temperature, it still experiences full relaxation. The relaxation time for 117°C is 3 minutes and 18 seconds by Equation 13. After the heat treatment, some pieces that accidentally came into contact with one another were lightly stuck together, implying there had been relaxation so as to fuse pieces in contact. There was also some warping, which makes sense, given that the pieces far exceeded their glass transition temperature. After testing the five pieces for each of these treatments and infill orientations, data were recorded, converted to force (with $g = 9.81 m/s^2$), divided by the cross sectional area, 4.99 mm^2, and then converted to MPa, see Figure 19.

Control	0° tensile strength (MPa)	45° tensile strength (MPa)	90° tensile strength (MPa)
1	35.426	34.512	32.123
2	34.679	37.736	30.590
3	32.802	32.251	34.099
4	33.313	35.013	34.463
5	34.207	35.308	31.258
Average	34.085	34.964	32.507

Full	0° tensile strength (MPa)	45° tensile strength (MPa)	90° tensile strength (MPa)
1	32.988	34.207	35.927
2	30.757	35.259	34.748

3	26.648	35.603	34.374
4	30.570	35.053	33.106
5	32.251	36.301	33.735
Average	30.643	35.285	34.378

Figure 19 - The results of tensile testing for the control group and the experimental heat treatment ('Full') group. Recall that 0^o is infill in the direction of the pull, 90^o is infill orthogonal to the pull, and 45^0 is 45^o from the direction of pull (Figure 12). It is important to note that the 0^o and 90^o samples test only tensile strength while 45^o samples include some of the other material properties like flexural modulus, given the more complex structure.

As seen from Figure 19, there is a notable change between the control group and the treated group and also between different infill orientations. The control group generally aligns well with the idea that alignment of the infill with the direction of pull produces higher tensile strength; however, unexpectedly 45^o infill pieces outperformed other pieces both in the control group and after the heat treatment. The large improvement seen in the 90^o test pieces strongly supports the hypothesis that further polymer entanglement between layers has a strong impact on tensile strength. A Student's *t*-test showed that at a significance threshold of 0.05 there is a significant difference between the 90^o control pieces and the 90^o treated pieces. Similarly, increases in the tensile strength of 45^o pieces supports this conclusion; however, there is strangely a sharp decline of tensile strength for 0^o pieces. A Student's *t*-test also showed that there is a significant change between the 0^o control pieces and the 0^o treated pieces (at the same significance threshold). Heat distribution in the pan used for heating wasn't entirely equal, and some of those pieces did have some partially melted areas, which may have caused the lowered tensile strength. It is also possible that there is some reverse diffusion force, which while insignificant when bonding surfaces together can cause previously homogenous PLA to slowly separate with heat. Error in the testing set up could also be at fault for this trend. More testing is certainly needed to assure accuracy. Still the observed results do strongly support the conclusion that polymer entanglement has a positive and important effect on the tensile strength of PLA. In fact, even this simple treatment caused a 5.8% increase in tensile strength for 90^o pieces on average. Additionally, Monoprice reports the tensile strength of their PLA+ product is 60 MPa

[42], suggesting that there may be more improvement possible. It is also important to recall that, due to the small size of samples, the outline, which is always in the direction of the pull, constituted a significant part of the piece, and this dampened the observed change. This could be resolved with larger test pieces and a stronger testing apparatus to accommodate greater forces.

Conclusions

These simulations yielded rather accurate behavior especially with regard to the verification of molecular weight dependence. While not ready to calculate relaxation times for polymer melts, the model does give meaningful insight into the adjacent problem of PLA relaxation in isolation without electrostatic interactions. It shows notably how this altered scope retains much of the same fundamental behavior and trends, and the notable differences possibly give insight into less polar polymers, where charge is less prominent, or even possibly in polymeric solutions where low concentrations of polymer essentially mean isolation for individual polymers (albeit with some solvent). Additionally, animations of polymer movement, while not analyzed in this investigation, can give more direct insight into the mechanisms of entanglement and what changes might be made to better support this process. Moreover, these simulations effectively demonstrate the similarities and differences between PLA in a polymer melt and the isolated PLA under exclusively Lennard Jones pair potentials. This model also serves as an excellent basis for further optimization and investigation of PLA, as with refinement of background and potentials, it is likely the observed difference can be reduced.

This model as a whole is very useful in further investigations concerning a variety of applications. First, functionalization (or the changing of functional groups on the monomers, e.g. replacing a methyl group with an ethyl group) is relatively easy with the scripts written in this project, and with minor changes, different chemistries could be analyzed. This is important as often functionalizing in a lab context is difficult and costly, while simulations can provide the groundwork and suggest which functional changes to investigate further in the lab. Additionally, this model can aid in research on extreme conditions. High or low temperatures and pressures can be expensive and make obtaining data difficult. This model, with minor changes and improvements, could provide a valuable window into PLA (or other plastic) usage in these conditions. Finally, this model can aid in the study of polymers like PLA for coatings. Creating a boundary and characterizing the degree of adhesion to the surface is very feasible in LAMMPS and molecular dynamics in general and can, once more, preface and inform experimental design and goals. Thus, this model and associated scripts serve as important groundwork to this application as well. These promising initial results give a good idea of the possible impact and effectiveness of this model both in this investigation and in a wide variety of additional usages.

To the end of answering the original question "To what extent does polymer entanglement impact the tensile strength of PLA?", the material tensile tests and informed heat treatments were successful in demonstrating the role of polymer entanglement in supporting bonding and producing a higher tensile strength. While the results are preliminary, they show that the pieces generally improve with the heat treatment, and the 90° test pieces (with infill orthogonal to the pull direction) had their tensile strength increased by 5.8% as a result of the treatment, making them stronger than the untreated 0° samples (with infill in the pull direction). This demonstrates that the heat treatment can effectively 'rescue' bonded surfaces, bringing them all the way to the strength of homogenous PLA. This shows that different degrees of polymer entanglement cause the observed difference in tensile strength between the 0° and the 90° control samples. It is important to note that some uncertainty exists around the unexpected results of the treated 0° samples, and while some explanations exist, more testing is the only way to ascertain the true cause and determine its impact on the observed results.

As a final note, it also could be difficult and would need further study to implement this sort of heat treatment on an industrial scale with complex parts, as the material would be able to move and deform, being above its glass transition temperature. However, this understanding of the relaxation segmental dynamics can help inform optimization of 3D printing processes to improve the balance between strength and shape retention. For example, alternate procedures during the manufacturing process can improve polymer entanglement; e.g. if the printer dwells longer, it could provide the needed heat for a more complete relaxation during the print. Also, it is possible to conduct heat treatments more pragmatically in only locations of the part that need additional strength, though warping could become more of an issue.

Future Steps

Given more time, there are four major steps that would improve the accuracy and impact of this project, and one additional goal which could tie many of the parts of this project together.

The first is resolving the issues surrounding charge and coulombic/electrostatic force within LAMMPS. Charge and charge-based forces are very important for molecular interactions, and not including them likely caused a lot of the inaccuracy observed in the project. However, given the time limits, it was not possible to decipher why LigParGen, Yale's online database where files were obtained, produced molecule files which diverged, not producing meaningful output. A large amount of time was spent trying various modifications to the simulation parameters of LAMMPS in an attempt to achieve convergence to no avail, so unfortunately, there was little choice but to accept simple Lennard Jones interactions without any electrostatic forces. Figuring this issue out and including electrostatic forces would likely reduce a lot of the error observed in the simulations.

An additional change that would refine the accuracy of these simulations is to conduct them in a polymer melt background. As observed in the Validation section, the lack of this background was unphysical and may have contributed to error in the calculated relaxation time, as the polymer melt would add realistic friction which would slow dynamics. Given more time this would be an ideal starting goal, as with some modifications to the system files and a general condensation step to bring the polymer together, it would be feasible with the given resources.

Similarly but more broadly, determining the cause of generally varying results in the computation is a vital goal. Unfortunately, deducing the source(s) of this deviation was not possible in the time frame, as it was already difficult to achieve these results. These simulations took a lot of time and resources to complete, and understanding and utilizing the LAMMPS framework and physics required time for research and learning. It seems likely that the cause could be the lack of electrostatic forces and the nonrealistic background conditions, but other sources could also be contributing. For example, problematic thermostating in the simulation, errors in the extension algorithm, or even simple error accumulated in LAMMPS simulations could all be a part of the observed change. Given the complexity of LAMMPS and the specialized knowledge required for ideal usage, parsing this problem will take more time.

Refining the procedure for testing polymer entanglement would also be very helpful in assuring significant results and more concrete conclusions. This could be as simple as utilizing a tensile testing machine, a lab grade oven, and/or a higher quality printer with larger pieces. Given the limited materials available, the tests completed were unfortunately all that was possible, but certainly with more precision, more definitive results can be obtained, allowing for much broader conclusions and even specific procedure recommendations for industrial manufacturers.

The additional step would be going far enough to actually entangle PLA atomistically with LAMMPS and perform tensile tests within simulations, using its barostat functionality. This would allow the simulations to connect directly with the tensile strength observed in testing and give a concrete basis for developing procedures to improve that strength, whether those are heat treatments as explored in this project, or they are chemical additives, or even differing 3D printing procedures to better provide strength where needed. Following through and simulating this would also provide meaningful understanding of how the material fails, which would provide key insight into even more potential changes to prevent that failure. This model will be a tool for vital optimization of PLA, which is especially important rooting back to PLA's unique biodegradability and the importance of wide uptake and usage to prevent more release of harmful plastics waste.

With these steps completed, these simulations will no doubt provide a meaningful window into the nanostructure of PLA, allowing much finer tuning of manufacturing processes and wider implementation.

Acknowledgements

This work could not have been completed without the incredible support of UNM's Center for Advanced Research Computing and their Research Associate Professor Dr. Matthew Fricke, Dr. Michael Chandross of Sandia National Labs, and my parents. The first provided huge amounts of computational resources (some thousands of CPU days) and help learning how to work with Slurm and the HPC interface, which allowed all of the simulations shown here. Their generosity to allow this usage is immense, and they cannot be thanked enough. Dr. Chandross additionally paved the way for actually setting up the simulations, providing excellent mentorship in navigating the complexity of such a powerful tool as LAMMPS. From project planning to sorting out the finer details like the special bonds command and puzzling over the strange behavior of charge in LigParGen files, his help smoothed the process and prevented a lot of roadblocks from causing damage. My mom was instrumental in parsing some of the dense rheology and polymer dynamics papers and textbooks, and my dad helped get me unstuck when these programs were not cooperating. Without the generosity of all of these people both in their

time and in their computational resources, this project would not have been able to reach the depth it did.

Bibliography

1 - Dilberoglu, Ugur M., et al. "The Role of Additive Manufacturing in the Era of Industry 4.0." *Procedia Manufacturing*, vol. 11, no. 1, 2017, pp. 545–554, https://doi.org/10.1016/j.promfg.2017.07.148.

2 - Harun, W. S. W., et al. "A Review of Powdered Additive Manufacturing Techniques for Ti-6al-4v Biomedical Applications." *Powder Technology*, vol. 331, 15 May 2018, pp. 74–97, www.sciencedirect.com/science/article/abs/pii/S0032591018301931, https://doi.org/10.1016/j.powtec.2018.03.010.

3 -Delgado Camacho, Daniel, et al. "Applications of Additive Manufacturing in the Construction Industry – a Forward-Looking Review." *Automation in Construction*, vol. 89, May 2018, pp. 110–119, https://doi.org/10.1016/j.autcon.2017.12.031.

4 - Lipton, Jeffrey I., et al. "Additive Manufacturing for the Food Industry." *Trends in Food Science & Technology*, vol. 43, no. 1, May 2015, pp. 114–123, www.sciencedirect.com/science/article/abs/pii/S092422441500045X, https://doi.org/10.1016/j.tifs.2015.02.004.

5 - Gibson, Ian, et al. *Additive Manufacturing Technologies : 3D Printing, Rapid Prototyping, and Direct Digital Manufacturing*. New York, Ny, Springer New York, 2015, pp. 245–268.

6 - Shergill, Kietan, et al. "An Investigation into the Layer Thickness Effect on the Mechanical Properties of Additively Manufactured Polymers: PLA and ABS." *The International*

Journal of Advanced Manufacturing Technology, vol. 126, no. 7-8, 6 Apr. 2023, pp. 3651–3665, https://doi.org/10.1007/s00170-023-11270-y.

7 - Paul, Sumit. "Finite Element Analysis in Fused Deposition Modeling Research: A Literature Review." *Measurement*, vol. 178, June 2021, p. 109320, https://doi.org/10.1016/j.measurement.2021.109320.

8 - Bertocco, Alcide, et al. "Stress Relaxation Behavior of Additively Manufactured Polylactic Acid (PLA)." *Materials*, vol. 15, no. 10, 1 Jan. 2022, p. 3509, www.mdpi.com/1996-1944/15/10/3509, https://doi.org/10.3390/ma15103509.

9 - Taib, Nur-Azzah Afifah Binti, et al. "A Review on Poly Lactic Acid (PLA) as a Biodegradable Polymer." *Polymer Bulletin*, vol. 80, no. 2, 6 Mar. 2022, pp. 1179–1213, https://doi.org/10.1007/s00289-022-04160-y.

10 - Gravelle, Simon, et al. "A Set of Tutorials for the LAMMPS Simulation Package [Article V1.0]." *Living Journal of Computational Molecular Science*, vol. 6, no. 1, 2025, https://doi.org/10.33011/livecoms.6.1.3037. Accessed 9 Nov. 2025.

11- Steimel, Joshua. *Polymer Physics (Steimel)*. California State Polytechnic University, 28 Jan. 2025, pp. 36–44.

12 - LigParGen web server: An automatic OPLS-AA parameter generator for organic ligands. Dodda, L. S.;Cabeza de Vaca, I.; Tirado-Rives, J.; Jorgensen, W. L. Nucleic Acids Research, Volume 45, Issue W1, 3 July 2017, Pages W331-W336

13 - Mitsutake, Ayori, and Hiroshi Takano. "Relaxation Mode Analysis for Molecular Dynamics Simulations of Proteins." *Biophysical Reviews*, vol. 10, no. 2, 15 Mar. 2018, pp. 375–389, https://doi.org/10.1007/s12551-018-0406-7.

14 - Thimm, Wolfgang, et al. “An Analytical Relation between Relaxation Time Spectrum and Molecular Weight Distribution.” *Journal of Rheology*, vol. 43, no. 6, 1 Nov. 1999, pp. 1663–1672, https://doi.org/10.1122/1.551066.

15 - Williams, Malcolm L., et al.. The temperature dependence of relaxation mechanisms in amorphous polymers and other glass-forming liquids. J. Am. Chem. Soc. 1955;77:3701–3707. doi: 10.1021/ja01619a008.

16 - Patti, Antonella, et al. “Predicting the Printability of Poly(Lactide) Acid Filaments in Fused Deposition Modeling (FDM) Technology: Rheological Measurements and Experimental Evidence.” *ChemEngineering*, vol. 7, no. 1, 23 Dec. 2022, pp. 1–1, https://doi.org/10.3390/chemengineering7010001.

17 - Goldstein, Kathy. “3D Printing Is Enabling Mass Personalization in Manufacturing | Nota3D.” *Nota3d.com*, 22 Mar. 2024, nota3d.com/2024/03/22/3d-printing-is-enabling-mass-personalization-in-manufacturing/.

18 - Iftekar, Syed Fouzan, et al. “Advancements and Limitations in 3D Printing Materials and Technologies: A Critical Review.” *Polymers*, vol. 15, no. 11, 1 Jan. 2023, p. 2519, www.mdpi.com/2073-4360/15/11/2519, https://doi.org/10.3390/polym15112519.

19 - Narjess Hajilou, et al. “A Comparative Review on Biodegradation of Poly(Lactic Acid) in Soil, Compost, Water, and Wastewater Environments: Incorporating Mathematical Modeling Perspectives.” *AppliedChem*, vol. 5, no. 1, 30 Dec. 2024, pp. 1–1, https://doi.org/10.3390/appliedchem5010001.

20 - World Wildlife Fund Australia. “The Lifecycle of Plastics.” *wwf.org.au*, 2021, wwf.org.au/blogs/the-lifecycle-of-plastics/.

21 - Yoo, Andy B., et al. “SLURM: Simple Linux Utility for Resource Management.” *Job Scheduling Strategies for Parallel Processing*, 2003, pp. 44–60, https://doi.org/10.1007/10968987_3.

22 - A. Stukowski, Visualization and analysis of atomistic simulation data with OVITO - the Open Visualization Tool, Modelling Simul. Mater. Sci. Eng. 18 (2010), 015012

23 - J. D. Hunter, "Matplotlib: A 2D Graphics Environment", Computing in Science & Engineering, vol. 9, no. 3, pp. 90-95, 2007.

24 - Harris, Charles R., et al. “Array Programming with NumPy.” *Nature*, vol. 585, no. 7825, 16 Sept. 2020, pp. 357–362, www.nature.com/articles/s41586-020-2649-2, https://doi.org/10.1038/s41586-020-2649-2.

25 - Virtanen, Pauli, et al. “SciPy 1.0: Fundamental Algorithms for Scientific Computing in Python.” *Nature Methods*, vol. 17, no. 3, 3 Feb. 2020, pp. 261–272, www.nature.com/articles/s41592-019-0686-2.

26 - The Pandas Development Team. “Pandas-Dev/Pandas: Pandas.” *Zenodo (CERN European Organization for Nuclear Research)*, 18 Oct. 2019, https://doi.org/10.5281/zenodo.3509134.

27 - Marzuki, Afeeqa Puteri, et al. “Fabrication and Evaluation of PLA/PA-HA Filament for 3D Printing: Towards Trabecular Bone-Compatible Biomedical Applications.” *The International Journal of Advanced Manufacturing Technology*, vol. 141, no. 1-2, 14 Oct. 2025, pp. 891–908, https://doi.org/10.1007/s00170-025-16623-3.

28 - “Repeating Unit of Poly Lactic Acid (PLA).” *Chemistry Stack Exchange*, chemistry.stackexchange.com/questions/98191/repeating-unit-of-poly-lactic-acid-pla.

29 - "Force Fields and Interactions – Practical Considerations for Molecular Dynamics." *Computecanada.github.io*, computecanada.github.io/molmodsim-md-theory-lesson-novice/01-Force_Fields_and_Interactions/index.html.

30 - Banks, J.L., et al. "Integrated Modeling Program, Applied Chemical Theory (IMPACT)." Journal of Computational Chemistry 2005, 26, 1752

31 - Ahmed, Jannat, et al. "Molecular Dynamics Modeling of Thermal Conductivity of Several Hydrocarbon Base Oils." *Tribology Letters*, vol. 71, no. 2, 7 May 2023, https://doi.org/10.1007/s11249-023-01738-z.

32 - Maple, Jon, et al. "Derivation of Force Fields for Molecular Mechanics and Dynamics from Ab Initio Energy Surfaces." *Proc. Nati. Acad. Sci. USA*, vol. 85, 1988, pp. 5350–5354, www.pnas.org/doi/abs/10.1073/pnas.85.15.5350, https://doi.org/10.1073/pnas.85.15.5350.

33 - Wikipedia Contributors. "Ensemble (Mathematical Physics)." *Wikipedia*, Wikimedia Foundation, 14 July 2025, en.wikipedia.org/wiki/Ensemble_%28mathematical_physics%29.

34 - Mitsutake, Ayori, and Hiroshi, Takano. "Relaxation Mode Analysis for Molecular Dynamics Simulations of Proteins." *Biophysical Reviews*, vol. 10, no. 2, 15 Mar. 2018, pp. 375–389, https://doi.org/10.1007/s12551-018-0406-7.

35 - Beaucage, Greg. *Relaxations in Polymers and the Glass Transition*. University of Cincinnati Chemical and Materials Engineering, 18 Jan. 2024, www.eng.uc.edu/~beaucag/Classes/Properties/Polymer%20Physics%20Homework%202024/HW2_2024/UTK%20PhysChem-of-Polymers-parts-7.pdf.

36 - Kenan Tüfekci, et al. "Stress Relaxation of 3D Printed PLA of Various Infill Orientations under Tensile and Bending Loadings." *Journal of Applied Polymer Science*, vol. 140, no. 39, 18 July 2023, https://doi.org/10.1002/app.54463.

37 - Thingiverse.com. "Dog Bone Tensile Test Piece." *Thingiverse - Digital Designs for Physical Objects*, 2022, www.thingiverse.com/thing:5221121. Accessed 29 Mar. 2026.

38 - Iowa State University. "Nondestructive Evaluation Physics : Materials." *Www.nde-Ed.org*, www.nde-ed.org/Physics/Materials/Mechanical/StressStrain.xhtml.

39 - Dorgan, John R, et al. "Melt Rheology of Poly(Lactic Acid): Entanglement and Chain Architecture Effects." *Journal of Rheology*, vol. 43, no. 5, 1 Sept. 1999, pp. 1141–1155, https://doi.org/10.1122/1.551041.

40 - Yonggang Shangguan, et al. "New Insight into Time-Temperature Correlation for Polymer Relaxations Ranging from Secondary Relaxation to Terminal Flow: Application of a Universal and Developed WLF Equation." *Polymers*, vol. 9, no. 11, 2 Nov. 2017, pp. 567–567, https://doi.org/10.3390/polym9110567.

41 - Briassoulis, D. "An Overview on the Mechanical Behaviour of Biodegradable Agricultural Films." *Journal of Polymers and the Environment*, vol. 12, no. 2, Apr. 2004, pp. 65–81, https://doi.org/10.1023/b:jooe.0000010052.86786.ef.

42 - *Monoprice 3D Printing Filament Comparison Chart*. Monoprice, downloads.monoprice.com/files/flyers/Filament_Comparison_Chart_180416.pdf.